NASA Technical Paper 1630

Application of Coherence in Fan Noise Studies

Joseph R. Balombin

FEBRUARY 1980

NASA

NASA Technical Paper 1630

Application of Coherence in Fan Noise Studies

Joseph R. Balombin
Lewis Research Center
Cleveland, Ohio

National Aeronautics
and Space Administration

**Scientific and Technical
Information Office**

1980

Summary

A 50.8-centimeter (20-in.) diameter, single-stage fan was tested with and without an inflow control device in the NASA Lewis Research Center anechoic chamber. In this report, an alternative approach to inflow control devices is presented for obtaining sound pressure levels with reduced random turbulence effects. This alternative, a signal-processing technique called coherence analysis, was applied to tape-recorded microphone data.

During the test, fan speed was varied between 9000 and 17 000 rpm, and measurements were taken over the inlet quadrant sound field. Sound pressure data were obtained both from fixed far-field microphones and from a moving survey microphone. The component of the sound pressure that was coherent with the fan rotor speed, the coherent sound pressure, was determined by using a digital signal processor and was studied as a function of fan speed and microphone position.

In determining the effectiveness of the coherence analysis technique, the levels of tone sound power measured with the inflow control device and the levels obtained by coherent processing were compared with the levels obtained during baseline static operation. At subsonic speeds, for which the rotor-stator and rotor-alone noise sources were cut off, the inflow control device reduced the blade-passing-frequency (BPF) tone power level by about 6 decibels from the baseline level. Coherent processing reduced the tone level by about 11 decibels from the baseline level. A combination of coherent processing and inflow control reduced the power level by about 13 decibels at these subsonic speeds. When the rotor noise sources were cut on, coherent processing reduced BPF levels by a few decibels, but inflow control had a negligible effect.

Plots of coherent sound pressure level as a function of inlet angle clearly indicated lobe patterns at all speeds. Differences between the directivity pattern maximum and minimum ranged to 20 decibels. As the fan rotor-alone noise source was cut on at about 13 000 rpm, the differences between the coherent pressure levels and the total pressure levels became less. As speed was increased, the coherent and total pressure levels converged, beginning at the 90° angle and gradually extending forward to the other inlet angles.

Variations in BPF tone were observed and studied as a function of time. By means of continuous averaging and coherent processing, the coherent component of the measured sound pressure was determined and plotted against time for each fixed microphone. Two similar test runs were compared and found to have different sound pressure directivity patterns when averaged with 3-second integration times and the same sound pressure directivity pattern when averaged with 200-second integration times.

Introduction

In the last few years, many fan noise studies have focused on understanding the role of inlet turbulence and flow distortions in setting the observed sound pressure levels (refs. 1 to 6). The level of the blade-passing-frequency (BPF) tone generally determines the overall fan noise level, and this level can vary by several decibels depending on the particulars of the operation. To reduce the BPF level to that which might be expected during actual flight, inflow control techniques such as honeycomb screen devices, support-structure cleanup, and augmented airflow past the nacelle have been used (refs. 2, 6, and 7). Little information has been derived, unfortunately, on the exact effect of these flow modifications on the fan noise sources. The usual and simplest comparison between baseline and alternative configurations is the difference between measured sound pressure levels (SPL). This method of analysis, however, gives only a figure of merit for a particular change in operating configuration.

The present study attempts to obtain additional information. The coherence function can be used to reject from the signal the component of fan noise due to random flow disturbances and consequently to permit a more detailed study of the deterministic noise sources due to synchronous interaction of the blades with flow-field disturbances. To demonstrate the usefulness of the coherence analysis, the signal-processing technique was applied to data obtained during testing of a 50.8-centimeter (20-in.) diameter fan. This fan was operated over a range of speeds in an anechoic chamber at the NASA Lewis Research Center. During this study the fan was operated with an inflow control device designed to reduce inflow disturbances. The results from this configuration with inflow control as well as those from a baseline configuration (without inflow control) are presented.

Theory

To estimate the amount of change in fan noise caused by a change in fan inflow conditions, a procedure other than simple subtraction of measured sound levels is desirable. Another approach in analyzing fan noise would be to separate the measured tone levels into two components. One component results from short-time turbulent or random inflow disturbances interacting with a fan rotor, perhaps at a variable position. The second component results from interactions with fixed, spatial, mean flow variations. This deterministic rotor component may be caused by interactions either between the mean rotor wakes and the stators or the downstream struts or between the rotor and fixed inlet distortions. All these mechanisms produce sounds of the same frequencies. The task, then, is to separate the far-field-tone sound pressure levels into deterministic (synchronously coherent) and random components.

Measured far-field sound pressures were separated by using coherence analysis to obtain coherent power spectra. As the name implies, this function compares two varying signals in terms of their similarity, or coherence. The two signals used in this application were a rotor speed pulse and a far-field microphone signal. After a period of time averaging it would be expected that the pressure component that was coherent, or at a relatively constant phase angle with respect to the rotor angular position, would remain. The pressure component that was due to interaction with unsteady flow would be expected to continuously decrease with successive coherent averaging.

The mathematical representation of ordinary coherence $[\gamma_{xy}^2(f)]$ as a function of frequency is (ref. 8)

$$\gamma_{xy}^2(f) = \frac{|G_{xy}(f)|^2}{G_x(f)G_y(f)}$$

which yields a value between 0 and 1. The cross spectral density function $|G_{xy}(f)|^2$ is normalized by dividing it by the product of the two individual spectra $G_x(f)$ and $G_y(f)$. The coherence is 0 if x and y are unrelated and 1 if x and y are linearly related. At intermediate values of coherence, x and y are not linearly related or there are unaccounted-for additional inputs or outputs.

A useful application of coherence is the computation of the coherent spectrum. This is done by multiplying the coherence by the SPL spectrum to compute the coherent SPL spectrum; that is, $\text{CSPL} = 10 \log_{10} [\gamma_{xy}^2(f)|G_y(f)|^2]$. In the present application, the coherence between fan speed and microphone pressure was multiplied by the microphone SPL spectrum to produce those values of sound pressure due to the fan sources that were correlated with fan rotation. The difference between this value and that of the customarily obtained SPL spectrum is presumed to be the random tone component that results from interaction between the fan rotor and random flow disturbances.

A number of processing parameters were involved in obtaining the coherent spectrum level. Among these parameters were filter bandwidth, averaging time, number of samples, and delay times between the two signals. Because the microphone data were random, the choice of processing parameters influenced the estimates of spectral values. One objective in coherent processing is to choose the processing parameters so that reasonable statistical confidence is obtained. The previously mentioned processing parameters are examined here for their effects on the coherence results.

Delay time is discussed first. In the situation studied, the source event was the interaction between the fan rotor and the pressure and flow fields in its vicinity. The sound radiated from this continuous process appeared at the far-field microphones after an appropriate sound propagation or delay time. For the digital processing that was used to obtain coherence, the two channels of information were divided into sequential blocks that were subsequently processed. For optimal results the two data blocks that are compared should be synchronized with respect to the event taking place. By delaying the rotor speed signal by the propagation time, this requirement was satisfied for the reported results. If it were not satisfied, the results would be somewhat lower than they should have been. This bias error factor can be estimated (ref. 9) as approximately $[1 - (\tau_{offset}/T_{sample})]^2$ where τ_{offset} is the sound propagation time difference in the data channels and T_{sample} is the time length of the data evaluated in an single block or average.

A variation in fan speed can also cause errors and increase uncertainty. Because of the fixed frequency resolution of the coherence or coherent spectrum analyses, a given fan-tone frequency will be analyzed in a particular filter with bandwidth Δf. If the speed variations are large enough, this particular bandwidth Δf may not be sufficient, and the tone will sometimes appear in adjacent filter bands. Consequently, over long periods of time, large variations in tone frequency result in a bias error that reduces the value of the coherence in the

frequency band containing the average tone frequency.

The number of samples that are taken together to form the average coherence has a strong influence on the quality of the result. A single sample has a coherence of 1 at all frequencies (ref. 8, p. 195). As the number of averages is increased, the coherence for linearly unrelated data approaches zero. Linearly related data, at those frequencies at which they are related, can be processed to approach the true value of coherence after greater averaging. The estimated coherence range is approximately

$$\gamma^2 \pm \sqrt{\frac{2}{n}} \left(\frac{1-\gamma^2}{\gamma}\right)$$

where n is the number of degrees of freedom (twice the number of independent samples) (ref. 10). Table I (from ref. 11) contains more exact values for the 90 percent confidence limits over which the coherence and the coherent spectrum will vary for a given number of averages and a given level of measured coherence. (The values for the coherent spectrum in table I(b) assume negligible errors in the original spectrum.)

As shown by either the approximate expression or the table, the measured coherence value itself influences the confidence limits; lower values of coherence are particularly uncertain. The bandwidth of the tone filtering has a direct bearing on this uncertainty. Larger bandwidths include not only the tone, but increasing amounts of noise at frequencies around the tone frequency. Because the fan noise is compared with the fan speed harmonics through the speed signal, the additional noise at non-speed-related frequencies that would be included within a larger bandwidth directly reduces the coherence level. The corresponding level of the coherent spectrum is not necessarily reduced by this reduction of coherence level since the spectrum level in the filter band becomes correspondingly larger with the larger bandwidth. However, the confidence limits around the estimated value of the coherent spectrum do become greater. Figure 1 displays a number of coherence measurements obtained by processing BPF fundamental tone data from a particular microphone. Data taken at two speeds are displayed—data taken at less than the fan rotor-alone cuton speed (fig. 1(a)), and data taken at greater than the cuton speed (fig. 1(b)). In both cases, as the bandwidth was decreased, the coherence approached its true value, and the scatter in the measured values became less.

The last source of inaccuracy to be considered affects only the survey microphone. Inherent in the presentation of survey-microphone coherent pressure as a function of microphone angle is an error in spatial resolution. To obtain a continuous curve of pressure against angle, the data were continuously averaged. There was a resulting angular offset in the survey coherent tone directivity that can be compensated for by simply shifting the pattern by a few degrees. The smoothing of the pattern features cannot be compensated for, except by less averaging, which reduces the confidence level of the coherence estimate. The extent of the distortion due to smoothing, though probably not serious, is unknown. Since the low coherence values of the pattern minimums are particularly uncertain, improvement in spatial resolution would be difficult.

Procedures

Data were processed on a commercial two-channel digital signal processor. This unit has a resolution of 500 frequency points, with Kaiser-Bessel time weighting. In processing, the microphone pressure signal was delayed by the propagation time, filtered, and then multiplied by the filtered fan speed signal to derive the averaged cross-spectrum. This cross-spectrum was normalized by dividing by the product of the two averaged spectra to obtain the coherence. A total of 256 averages was generally used. The processing option chosen multiplied the coherence function by the sound pressure spectrum to compute the coherent SPL spectrum.

The fixed microphones were analyzed for coherence with frequency bandwidths of approximately 80 hertz, which generally was sufficient to contain excursions in tone frequency, at least for the fundamental BPF tone. Data from a moving (survey) microphone were processed by using bandwidths of 20 hertz for the blade passing frequency and 40 hertz for the second harmonic of the blade passing frequency (2BPF). In some instances, the filter widths for the survey microphone were not large enough; when that happened, the analysis was repeated for several filter bands and the final result for the coherent tone level was the maximum value at or near the nominal tone frequency. These particular selections of filter bandwidths were compromises between minimizing data scatter (fig. 1) and minimizing bias error due to speed variations during the averaging times that caused the tone frequency to vary between bands.

Equipment

Coherent processing was applied to data that were tape-recorded during fan tests in the Lewis anechoic chamber. The fan tested (ref. 12) was a

50.8-centimeter (20-in.) diameter, single-stage fan driven by a 7000-horsepower electric motor. The fan stage had 28 rotor blades and 59 stator vanes. Designated QF-12, this fan was tested from 9000 to 12 000 rpm, both with and without the inflow control device described in reference 2. Views of the fan inlet with and without the device are presented in figure 2.

The microphones used to obtain the pressure data were 0.62-centimeter (0.25-in.) diameter condenser microphones. Fixed-position microphones were located on a 7.6-meter (25-ft) radius arc around one inlet quadrant, on 10° spacing increments. The survey microphone moved along a similar arc, traversing the quadrant in approximately 200 seconds.

The speed signal with which the sound pressure was compared was a short pulse occurring once every revolution. Because of the narrowness of these fan speed pulses, there were harmonics at each multiple of the shaft passing frequency (SPF) (fig. 3). This spectrum feature of many harmonics permitted the coherence to be evaluated through many multiples of the revolution rate.

Results and Discussion

The results obtained during this study primarily concern the fan's blade passing frequency. Data were obtained, with and without inflow control, at 50, 60, 70, 75 (inflow control only), 80, and 90 percent of design speed. Microphones at fixed locations from 0° to 90° in 10° increments and a microphone that traversed this arc provided the sound pressure information.

The effect of coherent processing on the sound power spectrum is discussed first. The far-field pressure lobe patterns that existed around the inlet and their time variation are described later.

Sound Power Spectrum

Figures 4 to 8 present the sound power levels as a function of frequency for speeds of 50, 60, 70, 80, and 90 percent of design speed (corresponding to 9300, 11 100, 13 000, 14 900 and 16 800 rpm, respectively). The two upper curves of each figure represent the fan's sound power levels for operation in its baseline (standard) operating configuration and for operation with inflow control. The two bottom curves represent the coherent sound power levels for these same two configurations. The sound power levels were computed by adding the power contributions from all 10 fixed microphones located in the fan inlet quadrant. The greatest levels on these curves occur at the blade passing frequencies of the five speeds (~4300, 5100, 6000, 6900, and 7700 Hz). The small shifts in frequency between spectra at a particular speed are due to fan operation at corrected, rather than actual, speeds.

Particularly obvious in this series of figures is the large difference between the coherent power levels and the total power levels. In processing the data to obtain the coherent spectra, many coherent samples were averaged together. This averaging caused the reduction in random broadband levels. The reduction is a consequence of the lack of consistent phase agreement between the broadband sound pressure and the fan speed. Averaging reduced the incoherent levels by 10 log N decibels (ref. 13), where $N=256$ is the number of averages used in the present analysis. Thus the incoherent component was in this case reduced by about 24 decibels.

The blade passing and other shaft frequency multiples became more obvious in the coherent presentation since the large reduction in the incoherent broadband components accentuated the steady-phase fan interaction components. The remaining large scatter in the broadband levels after coherent processing reflects the large random error or uncertainty at these very small (<0.05) coherence values.

The small differences in coherent tone levels, with and without inflow control, are due partly to the uncertainty just mentioned and partly to variations that are discussed later. It was concluded that the coherent levels were hardly affected by the inflow control.

At the two highest speeds, 80 and 90 percent of design speed, multiple pure tones were present because of the cuton (ref. 14) of the rotor-alone pressure field. At the lower speeds the spectra changed only slightly from speed to speed. Between 70 and 85 percent of design speed both the rotor-alone noise source and the rotor-stator source at the blade passing frequency began to contribute, and these source contributions can be seen in the coherent power. The rotor-alone source was a result of the blade tips rotating at supersonic speed (~345 m/sec (1140 ft/sec) at 80 percent speed). Rotor-alone noise began to propagate at about 77 percent of design speed, the rotor-stator noise for the fundamental at about 85 percent speed. Finally, some blade shocks added to the level of several SPF harmonics. The net effect of these sources was an increase of about 15 decibels in the coherent spectral levels between 70 and 80 percent of design speed.

At the 90 percent speed (fig. 8) the coherent spectrum and the total spectrum are even closer in level than at 80 percent speed (fig. 7), particularly because the many coherent SPF multiples were

greatly increased. One other difference between speeds was that the levels of the BPF tone and its harmonics were lower at 90 percent speed than at 80 percent.

The preceding BPF tone results are summarized in figure 9, which presents the relative power level results from survey-microphone data. The reference for each point is the baseline data at each speed. Inflow control reduced power levels by 6 decibels at low speeds and somewhat less at higher speeds. The relatively positive 80-percent-speed point is probably an error in the baseline due to baseline unsteadiness. Coherent processing of the baseline data reduced the calculated power levels approximately 5 decibels below the inflow control levels, for a total reduction of 11 decibels from the baseline level. Coherent processing reduced the inflow control levels by 6 decibels at subsonic speeds and by 2 decibels at 80 percent speed and higher. Judging from the data at 80 and 90 percent speed, the relative amount of randomness in the tone became small enough that either coherent processing or inflow control was effective in reducing the tone to its coherent component.

Figure 10 presents the actual power levels for the fan's blade passing and second harmonic frequencies. Results are presented for these data after coherent processing on both the baseline testing and the testing with the inflow control device. These data, as well as those of the previous figure, were taken from survey-microphone results, not from the originally displayed power spectrum results from fixed microphones. The values of sound power from fixed and survey microphones are similar; but, because of directivity pattern minimums, the fixed-microphone results may appear erratic when a minimum coincides with a measurement location.

The data of figure 10 suggest that before cuton the coherent BPF tone increased approximately as the 6th power of the tip speed. As cuton was attained, the tone level increased quickly by almost 20 decibels over a 10-percent-speed range and then subsequently leveled off. The second harmonic, already cut on at low speeds, increased at the same approximately 20-decibel-per-octave slope throughout much of the speed range. As did the BPF tone, the 2BPF tone increased significantly at 80 percent speed, although the increase (due only to a rotor-alone contribution) was about half that of the BPF.

From the coherent power level trends with speed, some confirmation of the present understanding of fan noise sources is possible. The rotor-alone source is the only mechanism that can account for both the BPF and 2BPF tone increases. The BPF tone has the additional rotor-stator interaction source, which cuts on at about 85-percent speed and allows additional sound power to be generated and to propagate from the fan above that speed.

For these observations, coherent processing was particularly useful in uncovering the details of the power trends. The total power levels tend to vary too little with speed to enable any clear statements about the generated fan noise.

Directivity Pattern

Coherent processing shows the sound pressure to be spatially radiated in a clearly lobed pattern. Directivity patterns of the fan's BPF tone are presented at this point, and some of their characteristics are noted.

Figures 11 to 15 illustrate the survey-microphone BPF tone directivity patterns for 50, 60, 70, 80, and 90 percent of design speed. As before, the fan was operating in either its baseline or inflow control configuration. On each figure there are three curves. The upper curve is the directivity pattern of the BPF tone for the baseline configuration. The middle curve is the directivity pattern of the BPF tone with the fan operating with the inflow control device. The lower curve is the coherent BPF directivity pattern obtained from the baseline data. The value of the coherence itself for the lower curve data typically ranges from 0.05 to 0.25. This fraction, when multiplied by the total sound pressure level of the blade passing frequency, as indicated by the upper curve, results in a value of coherent sound pressure approximately 5 to 20 decibels less than the total of coherent and incoherent components. The low-speed reductions in level obtained by simply operating the fan with inflow control to reduce turbulence are rather independent of angle. Judging from the level of the inflow control curve, in relation to the coherent data curve, there seems to be good confirmation of the common understanding that reducing inflow turbulence reduces a random component of the BPF tone.

On examination of the coherent data, it is evident that pressure lobes exist at all speeds, regardless of whether rotor-alone or rotor-stator sound generation modes are propagated. As previously noted, these curves, rather than the fixed-microphone data, were used to obtain the power results in figures 9 and 10. The poorer angular resolution of the fixed microphones makes it difficult to properly detect these pressure lobes. The lobes generally have widths of only about 20°, with minimum values approximately 10 decibels less than the maximum values.

As was the case for the power curves (figs. 4 to 6), the 50-, 60-, and 70-percent-speed pressure data (figs. 11 to 13) show a clear division between base-

line, inflow control, and coherent baseline curves. For the 80- and 90-percent-speed pressure data (figs. 14 and 15), some crossovers do occur. The coherent baseline, by definition, is always a value less than, or equal to, the baseline value. The inflow control data, however, do not always fall between the limits of the baseline and coherent baseline data at the 80 and 90 percent speeds. In addition to this difference for the inflow control configuration data, at 90 percent speed, the inflow control directivity pattern seems to differ from that of the baseline data. One reason for this difference is a BPF-tone time variation.

This time variation is demonstrated in figure 16, where the directivity patterns for the coherent BPF tone level are compared for two 90-percent-speed runs. The fan was operated in its baseline configuration, and the data from the two runs were recorded within a minute of each other so that the speed setting was not changed. So that the relative confidence level of these data can be appreciated, the 90 percent confidence levels (from table 1) surrounding these data have been included. Although the data for the two runs may be the same at some angles, it is apparent that the directivity patterns are different.

Time histories for these two 90-percent-speed, baseline-condition runs are presented in figure 17. These coherent BPF tone data are continuous 3-second averages from fixed-position microphones, 0° to 90°, with each angle's data offset by 15 decibels to avoid confusion. Time and SPL scales are indicated for the series of curves. These time histories demonstrate long-term variations of several decibels, over periods of 1 to 2 minutes. This figure suggests strong similarities between the results for adjacent microphones, particularly for 0° and 10° as one group and 60° to 90° as another. These particular angles form lobes in the far-field pressure, as indicated by the directivity curves of figures 15 and 16. Fairly long-term variations, or amplitude modulations in the pressure level, as illustrated in figure 17, would cause differences in the levels and apparent widths of the pressure lobes as a function of time. These changes would be sufficient to account for the observed crossover between inflow control and coherent baseline data of figures 14 and 15. These relatively long-term pressure variations may be a result of turbulent eddies in the inflow interacting with the fan rotor.

The run 243 and run 245 time histories of figure 17 were averaged, and these two runs were again compared, as shown in figure 18. The only differences between figure 16 and figure 18 are that the figure 18 data were obtained from fixed microphones rather than the survey microphone and were averaged over much longer times—200 seconds rather than about 3 seconds. The good agreement in figure 18 between the data of the two consecutive test runs confirms the similarity of the average directivity patterns for 200-second averaging time.

Another example of the time variation of the coherent tone level is presented in figure 19. In this example, 50-percent-speed, coherent BPF level data are presented. The format is the same as that of figure 17. A 2-minute-long variation clearly took place at the 50°, 60°, and 70° microphone positions. At about 2 to 2.5 minutes into the record, the coherence at 60° and 70° became nearly zero and this caused the low and highly uncertain coherent pressure levels. As for the 90-percent-speed data, some uncertainty in the survey-microphone coherent pressure directivity patterns is probably due to time variations.

Over short periods of time, the coherent or rotor-locked component of the blade passing frequency changed by several decibels, as illustrated in figures 17 and 19. It is interesting that this component is not constant with time and that the pattern of changes seems to hold even for adjacent microphones. Since the directivity patterns that correspond to these time-history traces result from rotor interaction modes, there apparently is no one particular mode pattern always present. Averaging over long periods of time reveals a consistent directivity pattern and the existence of a mean mode distribution. It is not clear what would account for the dynamic changes in fan mode distribution and for similar behavior for cuton (90 percent) and cutoff (50 percent) speeds. A spatial movement of an inflow disturbance pattern in the radial or circumferential direction could produce shifts in source mode content and account for some of the observed directivity changes if the observed pressure lobes were due to mode orders.

Concluding Remarks

In the preceding discussion, applications of the coherence function to fan noise have been presented. By computing the coherence between the sound pressure signal from a far-field microphone and the speed signal from the fan, the component of the blade-passing-frequency (BPF) tone due to steady (spatially fixed) rotor interactions and interactions with very low-frequency flow disturbances can be determined. This level, given by the coherent power spectrum, approaches the total BPF tone level at fan speeds greater than the rotor-alone cuton speed. In addition, the far-field coherent sound pressure variation with inlet angle shows distinct lobes 20° to 30° wide that appear to be

modulated in level over periods as long as 2 minutes.

These results were obtained with fan rotational speed as the reference signal for coherence computation and frequency domain processing. An internal sound pressure level could have been used as an alternative reference signal; but, because that pressure would itself have been a function of the fan inflow disturbance pattern, it could not be as easily used to obtain the synchronous component of noise. Increased averaging removed higher frequency interactions, thereby converging on steady rotor-tone noise. Processing as a function of frequency, which isolated tones, was also an advantage in that it permitted the pressure-lobe time variations to be easily detected.

Some comparison was made between results of the fan-tone levels from the fan operating with and without an inflow control device (designed to reduce inlet turbulence). Sound pressure levels associated with a fan operated with inflow control are less than those of a fan operated without inflow control and greater than those of the typical operation after coherent data processing. Since the coherent tone results are freer of random turbulence effects than the inflow control results, it would seem possible to simply apply coherent processing to fan-tone noise data to obtain results that would approach flyover character. The extent of the agreement between flyover data and data coherently processed in a static test facility would remain somewhat a function of the facility because of possible fixed distortions in a test facility, the effects of which are not removed by this coherence technique.

Lewis Research Center,
National Aeronautics and Space Administration,
Cleveland, Ohio, August 30, 1979,
505-03.

References

1. Feiler, C. E.; and Merriman, J. E.: Effects of Forward Velocity and Acoustic Treatment on Inlet Fan Noise. AIAA Paper 74-946, Aug. 1974.
2. Shaw, L. M., et al.: Inlet Turbulence and Fan Noise Measured in an Anechoic Wind Tunnel and Statically with an Inlet Flow Control Device. NASA TM-7323, 1977. (Also AIAA Paper 77-1345, Oct. 1977.)
3. Hanson, D. B.: Measurements of Static Inlet Turbulence. AIAA Paper 75-467, Mar. 1975.
4. Bekofske, K. L.; Sheer, R. E.; and Wang, J. C. F.: Fan Inlet Disturbances and Their Effect on Static Acoustic Data. ASME Paper 77-GT-63, Mar. 1977.
5. Robbins, B.; and Lakshminarayana, B.: Effect of Inlet Turbulence on Compressor Noise. J. Aircr., vol. 11, no. 5, May 1974, pp. 273-281.
6. Feiler, C. E.; and Groeneweg, J. F.: Summary of Forward Velocity Effects on Fan Noise. NASA TM-73722, 1977. (Also AIAA Paper 77-1319, Oct. 1977.)
7. Heidmann, M. F.; and Dietrich, D. A.: Simulation of Flight-Type Engine Fan Noise in the NASA Lewis 9x15 Anechoic Wind Tunnel. NASA TM-73540, 1976.
8. Bendat, J. S.; and Piersol, A. G.: Random Data: Analysis and Measurement Procedures. John Wiley & Sons, Inc., 1971.
9. Seybert, A. F.; and Hamilton, J. F.: Time Delay Bias Errors in Estimating Frequency Response and Coherence Functions. J. Sound Vibr., vol. 60, no. 1, Sept. 1978, pp. 1-9.
10. Bendat, J. S.: Statistical Errors in Measurement of Coherence functions and Input/Output Quantities. J. Sound Vibr., vol. 59, no. 3, Aug. 1978, pp. 405-421.
11. Karchmer, A. M.: Identification and Measurement of Combustion Noise from a Turbofan Engine Using Correlation and Coherence Techniques. NASA TM-73747, 1977. (Also Ph.D. Thesis, Case Western Reserve University, 1978.)
12. Lucas, J. G.; Woodward, R. P.; and MacKinnon, M. F.: Acoustic Evaluation of a Novel Swept-Rotor Fan. NASA TM-78878, 1978. (Also AIAA Paper 78-1121, July 1978.)
13. Pendergrass, N. A.: Coherence Function and Averaging Boost Confidence in Spectrum Measurements. Electronics, vol. 51, no. 19, Sept. 14, 1978, pp. 132-137.
14. Tyler, J. M.; and Sofrin, T. G.: Axial Flow Compressor Noise Studies. SAE Trans., vol. 70, 1962, pp. 309-332.

TABLE I. - 90 PERCENT CONFIDENCE LIMITS

(a) On coherence function measured with average of N samples

Measured coherence	Number of samples, N								
	16	32	64	128	256	512	1024	2048	4096
	Confidence limits								
0.01	----------	----------	----------	----------	0.000-.027	0.002-.022	0.004-.018	0.005-.016	0.007-.014
.02	----------	----------	----------	----------	.004-.043	.008-.036	.011-.031	.013-.028	.015-.025
.03	----------	----------	----------	0.004-.069	.009-.057	.015-.049	.019-.043	.022-.039	.024-.036
.04	----------	----------	----------	.008-.083	.016-.070	.022-.061	.027-.055	.031-.050	.033-.047
.05	----------	----------	0.004-.118	.013-.097	.022-.083	.030-.073	.035-.066	.039-.061	.042-.058
.06	----------	----------	.008-.132	.019-.111	.029-.095	.038-.085	.044-.077	.048-.072	.052-.069
.07	----------	----------	.012-.146	.025-.123	.037-.107	.046-.096	.053-.088	.058-.083	.061-.079
.08	----------	0.003-.192	.017-.160	.032-.136	.045-.119	.054-.108	.062-.099	.067-.094	.071-.090
.09	----------	.005-.206	.022-.173	.039-.148	.052-.131	.063-.119	.071-.110	.076-.104	.080-.100
.10	----------	.008-.220	.028-.185	.046-.160	.061-.142	.072-.130	.080-.121	.086-.115	.090-.110
.11	----------	.012-.233	.033-.198	.053-.172	.069-.154	.080-.141	.089-.132	.095-.125	.099-.121
.12	----------	.016-.246	.040-.210	.061-.184	.077-.165	.089-.152	.098-.142	.104-.136	.109-.131
.13	----------	.020-.259	.046-.222	.069-.195	.086-.176	.098-.163	.107-.153	.114-.146	.119-.141
.14	----------	.025-.271	.053-.234	.076-.207	.094-.187	.107-.173	.117-.164	.124-.157	.128-.152
.15	0.003-.333	.030-.283	.060-.245	.085-.218	.103-.198	.117-.184	.126-.174	.133-.167	.138-.162
.16	.005-.345	.035-.295	.067-.257	.093-.229	.112-.209	.126-.195	.136-.184	.143-.177	.148-.172
.17	.008-.357	.041-.306	.075-.268	.101-.240	.121-.220	.135-.205	.145-.195	.152-.188	.158-.182
.18	.011-.369	.047-.318	.082-.279	.110-.251	.130-.230	.144-.216	.155-.205	.162-.198	.167-.193
.19	.014-.380	.053-.329	.090-.290	.118-.262	.139-.241	.154-.226	.164-.216	.172-.208	.177-.203
.20	.018-.392	.060-.340	.098-.301	.127-.272	.148-.251	.163-.237	.174-.226	.182-.218	.187-.213
.21	.022-.403	.066-.351	.106-.312	.136-.283	.157-.262	.173-.247	.184-.236	.191-.229	.197-.223
.22	.026-.413	.073-.362	.114-.323	.144-.293	.167-.272	.182-.257	.193-.246	.201-.239	.207-.233
.23	.031-.424	.080-.372	.122-.333	.153-.304	.176-.283	.192-.268	.203-.257	.211-.249	.217-.243
.24	.035-.435	.088-.383	.131-.344	.163-.314	.185-.293	.201-.278	.213-.267	.221-.259	.226-.253
.25	.041-.445	.095-.393	.139-.354	.172-.325	.195-.303	.211-.288	.223-.277	.231-.269	.236-.264
.26	.046-.455	.103-.404	.148-.364	.181-.335	.204-.314	.221-.298	.232-.287	.240-.279	.246-.274
.27	.052-.465	.111-.414	.157-.374	.190-.345	.214-.324	.230-.308	.242-.297	.250-.289	.256-.284
.28	.058-.475	.119-.424	.166-.385	.200-.355	.223-.334	.240-.318	.252-.307	.260-.299	.266-.294
.29	.064-.485	.127-.434	.175-.395	.209-.365	.233-.344	.250-.329	.262-.317	.270-.309	.276-.304
.30	.071-.494	.135-.444	.184-.405	.219-.375	.243-.354	.260-.339	.272-.327	.280-.320	.286-.314
.31	.077-.504	.144-.453	.193-.415	.228-.385	.253-.364	.270-.349	.282-.338	.290-.330	.296-.324
.32	.084-.513	.152-.463	.202-.424	.238-.395	.262-.374	.280-.359	.292-.348	.300-.340	.306-.334
.33	.092-.522	.161-.473	.212-.434	.248-.405	.272-.384	.290-.369	.302-.358	.310-.350	.316-.344
.34	.099-.531	.170-.482	.221-.444	.257-.415	.282-.394	.300-.379	.312-.367	.320-.360	.326-.354
.35	.107-.540	.179-.491	.231-.453	.267-.425	.292-.404	.309-.389	.322-.377	.330-.370	.336-.364
.36	.115-.549	.188-.501	.241-.463	.277-.435	.302-.414	.319-.398	.332-.387	.340-.379	.346-.374
.37	.123-.558	.198-.510	.251-.473	.287-.444	.312-.424	.330-.408	.342-.397	.350-.369	.356-.384
.38	.131-.567	.207-.519	.260-.482	.297-.454	.322-.433	.340-.418	.352-.407	.360-.399	.366-.394
.39	.139-.576	.217-.528	.270-.492	.307-.464	.332-.443	.350-.428	.362-.417	.370-.409	.376-.404
.40	.148-.584	.226-.537	.280-.501	.317-.473	.342-.453	.360-.438	.372-.427	.380-.419	.386-.414
.41	.157-.593	.238-.548	.292-.511	.328-.483	.353-.463	.370-.448	.382-.437	.390-.429	.396-.424
.42	.166-.601	.248-.557	.302-.520	.338-.493	.363-.472	.380-.458	.392-.447	.400-.439	.406-.434
.43	.175-.609	.258-.566	.312-.530	.348-.502	.373-.482	.390-.467	.402-.457	.410-.449	.416-.443
.44	.185-.618	.268-.575	.322-.539	.359-.512	.384-.492	.401-.477	.412-.466	.421-.459	.426-.453
.45	.195-.626	.279-.583	.333-.548	.369-.521	.394-.501	.411-.487	.423-.476	.431-.469	.436-.463
.46	.204-.634	.289-.592	.343-.557	.380-.530	.404-.511	.421-.496	.433-.486	.441-.479	.447-.473
.47	.215-.642	.300-.600	.354-.566	.390-.540	.415-.520	.431-.506	.443-.496	.451-.488	.457-.483
.48	.225-.650	.310-.609	.364-.575	401-.549	.425-.530	.442-.516	.453-.506	.461-.498	.467-.493
.49	.235-.658	.321-.617	.375-.584	.411-.558	.435-.539	.452-.525	.463-.515	.471-.508	.477-.503
.50	.246-.666	.332-.626	.386-.593	.422-.568	.446-.549	.462-.535	.474-.525	.481-.518	.587-.513

TABLE I. - Continued.

(a) Concluded

Measured coherence	Number of samples, N								
	16	32	64	128	256	512	1024	2048	4096
	Confidence limits								
0.51	0.257-.673	0.343-.634	0.397-.602	0.432-.577	0.456-.558	0.473-.545	0.484-.535	0.492-.528	0.497-.523
.52	.268-.681	.354-.642	.408-.610	.443-.586	.467-.568	.483-.554	.494-.544	.502-.537	.507-.532
.53	.279-.689	.365-.651	.419-.619	.454-.595	.477-.577	.493-.564	.504-.554	.512-.547	.517-.542
.54	.290-.696	.376-.659	.430-.628	.465-.604	.488-.586	.504-.573	.515-.564	.522-.557	.528-.552
.55	.302-.704	.387-.667	.441-.637	.475-.613	.499-.596	.514-.583	.525-.574	.532-.567	.538-.562
.56	.313-.711	.399-.675	.452-.645	.486-.622	.509-.605	.525-.592	.535-.583	.543-.577	.548-.572
.57	.325-.719	.411-.683	.463-.654	.497-.631	.520-.614	.535-.602	.546-.593	.553-.586	.558-.582
.58	.337-.726	.422-.691	.474-.662	.508-.640	.530-.624	.546-.611	.556-.603	.563-.596	.568-.591
.59	.350-.734	.434-.699	.486-.671	.519-.649	.541-.633	.556-.621	.566-.612	.573-.606	.578-.601
.60	.362-.741	.446-.707	.497-.680	.530-.658	.552-.642	.567-.630	.577-.622	.584-.616	.589-.611
.61	.375-.748	.458-.715	.509-.688	.541-.667	.563-.652	.577-.640	.587-.631	.594-.625	.599-.621
.62	.387-.755	.470-.723	.520-.697	.552-.676	.573-.661	.588-.649	.598-.641	.604-.635	.609-.631
.63	.400-.762	.482-.731	.532-.705	.563-.685	.584-.670	.598-.659	.608-.651	.615-.645	.619-.640
.64	.413-.770	.494-.739	.543-.713	.575-.694	.595-.679	.609-.668	.618-.660	.625-.654	.629-.650
.65	.427-.777	.507-.747	.555-.722	.586-.703	.606-.688	.619-.678	.629-.670	.635-.644	.640-.660
.66	.440-.784	.519-.754	.567-.730	.597-.712	.617-.697	.630-.687	.639-.679	.645-.674	.650-.670
.67	.454-.791	.532-.762	.579-.739	.608-.720	.628-.707	.641-.696	.650-.689	.656-.684	.660-.680
.68	.467-.798	.545-.770	.591-.747	.620-.729	.639-.716	.651-.706	.660-.699	.666-.693	.670-.689
.69	.481-.804	.557-.777	.603-.755	.631-.738	.650-.725	.662-.715	.671-.708	.676-.703	.680-.699
.70	.496-.811	.570-.785	.615-.763	.642-.747	.661-.734	.673-.725	.681-.718	.687-.713	.691-.709
.71	.510-.818	.583-.792	.627-.772	.654-.755	.672-.743	.683-.734	.692-.727	.697-.722	.701-.719
.72	.524-.825	.596-.800	.639-.780	.665-.764	.683-.752	.694-.743	.702-.737	.707-.732	.711-.728
.73	.539-.831	.610-.808	.651-.788	.677-.773	.694-.761	.705-.752	.713-.746	.718-.742	.721-.738
.74	.554-.838	.623-.815	.663-.796	.688-.781	.705-.770	.716-.762	.723-.756	.728-.751	.732-.748
.75	.569-.845	.636-.822	.675-.804	.700-.790	.716-.779	.726-.771	.734-.765	.739-.761	.742-.758
.76	.584-.851	.650-.830	.688-.812	.712-.799	.727-.788	.737-.780	.744-.775	.749-.770	.752-.767
.77	.599-.858	.663-.837	.700-.820	.723-.807	.738-.797	.748-.790	.755-.784	.759-.780	.763-.777
.78	.615-.864	.677-.845	.713-.828	.735-.816	.749-.806	.759-.799	.765-.794	.770-.790	.773-.787
.79	.631-.871	.690-.852	.725-.836	.747-.824	.760-.815	.770-.808	.776-.803	.780-.799	.783-.797
.80	.646-.877	.704-.859	.738-.844	.758-.833	.772-.824	.780-.817	.786-.812	.791-.809	.793-.806
.81	.662-.884	.718-.867	.750-.852	.770-.841	.783-.833	.791-.827	.797-.822	.801-.819	.804-.816
.82	.679-.890	.732-.874	.763-.860	.782-.850	.794-.842	.802-.836	.808-.831	.811-.828	.814-.826
.83	.695-.897	.746-.881	.776-.868	.794-.858	.805-.851	.813-.845	.818-.841	.822-.838	.824-.836
.84	.712-.903	.761-.888	.789-.876	.806-.867	.817-.860	.824-.854	.829-.850	.832-.847	.835-.845
.85	.728-.909	.775-.895	.801-.884	.818-.875	.828-.868	.835-.863	.839-.860	.843-.857	.845-.855
.86	.745-.915	.789-.903	.814-.892	.830-.884	.839-.877	.846-.873	.850-.869	.853-.866	.855-.865
.87	.762-.922	.804-.910	.827-.900	.841-.892	.851-.886	.857-.882	.861-.878	.864-.876	.865-.874
.88	.780-.928	.818-.917	.840-.908	.853-.901	.862-.895	.868-.891	.871-.888	.874-.886	.876-.884
.89	.797-.934	.833-.924	.853-.915	.866-.909	.873-.904	.879-.900	.882-.897	.884-.895	.886-.894
.90	.815-.940	.848-.931	.866-.923	.878-.917	.885-.913	.890-.909	.893-.907	.895-.905	.896-.903
.91	.832-.946	.862-.938	.879-.931	.890-.926	.896-.921	.901-.918	.903-.916	.905-.914	.907-.913
.92	.850-.952	.877-.945	.893-.939	.902-.934	.908-.930	.912-.927	.914-.925	.916-.924	.917-.923
.93	.868-.958	.892-.952	.906-.946	.914-.942	.919-.939	.923-.937	.925-.935	.926-.933	.927-.932
.94	.887-.964	.908-.959	.919-.954	.926-.951	.931-.948	.934-.946	.936-.944	.937-.943	.938-.942
.95	.905-.970	.923-.966	.933-.962	.938-.959	.942-.956	.945-.955	.946-.953	.947-.952	.948-.952
.96	.924-.976	.938-.973	.946-.970	.951-.967	.954-.965	.956-.964	.957-.963	.958-.962	.959-.961
.97	.943-.982	.953-.979	.959-.977	.963-.975	.965-.974	.967-.973	.968-.972	.968-.971	.969-.971
.98	.961-.988	.969-.986	.973-.985	.975-.984	.977-.983	.978-.982	.978-.981	.979-.981	.979-.981
.99	.981-.994	.984-.993	.986-.992	.988-.992	.988-.991	.989-.991	.989-.991	.989-.990	.990-.990

TABLE I. - Continued.

(b) On coherence output power spectrum computed by means of coherence function measured with average of N samples

Measured coherence	Number of samples, N								
	16	32	64	128	256	512	1024	2048	4096
	Confidence level, dB								
0.01	----------	----------	----------	----------	-13.3/+4.4	-6.8/+.3.4	-4.1/+2.6	-2.6/+1.9	-1.8/+1.4
.02	----------	----------	----------	----------	-6.8/+3.3	-4.1/+2.5	-2.6/+1.9	-1.8/+1.4	-1.2/+1.0
.03	----------	----------	----------	-8.9/+3.6	-5.0/+2.8	-3.1/+2.1	-2.1/+1.6	-1.4/+1.1	-1.0/+0.8
.04	----------	----------	----------	-6.9/+3.2	-4.1/+2.4	-2.6/+1.8	-1.7/+1.4	-1.2/+1.0	-0.8/+0.7
.05	----------	----------	-10.8/+3.7	-5.7/+2.9	-3.5/+2.2	-2.3/+1.6	-1.5/+1.2	-1.0/+0.9	-0.7/+0.6
.06	----------	----------	-8.9/+3.4	-5.0/+2.7	-3.1/+2.0	-2.0/+1.5	-1.4/+1.1	-0.9/+0.8	-0.6/+0.6
.07	----------	----------	-7.7/+3.2	-4.4/+2.5	-2.8/+1.9	-1.8/+1.4	-1.2/+1.0	-0.8/+0.7	-0.6/+0.5
.08	----------	----------	-6.8/+3.0	-4.0/+2.3	-2.5/+1.7	-1.7/+1.3	-1.1/+0.9	-0.8/+0.7	-0.5/+0.5
.09	----------	-12.4/+3.6	-6.1/+2.8	-3.7/+2.2	-2.3/+1.6	-1.6/+1.2	-1.1/+0.9	-0.7/+0.6	-0.5/+0.5
.10	----------	-10.8/+3.4	-5.6/+2.7	-3.4/+2.0	-2.2/+1.5	-1.4/+1.1	-1.0/+0.8	-0.7/+0.6	-0.5/+0.4
.11	----------	-9.7/+3.3	-5.2/+2.5	-3.2/+1.9	-2.0/+1.5	-1.4/+1.1	-0.9/+0.8	-0.6/+0.6	-0.4/+0.4
.12	----------	-8.8/+3.1	-4.8/+2.4	-3.0/+1.8	-1.9/+1.4	-1.3/+1.0	-0.9/+0.7	-0.6/+0.5	-0.4/+0.4
.13	----------	-8.1/+3.0	-4.5/+2.3	-2.8/+1.8	-1.8/+1.3	-1.2/+1.0	-0.8/+0.7	-0.6/+0.5	-0.4/+0.4
.14	----------	-7.5/+2.9	-4.2/+2.2	-2.6/+1.7	-1.7/+1.3	-1.2/+0.9	-0.8/+0.7	-0.5/+0.5	-0.4/+0.3
.15	-16.6/+3.5	7.0/+.2.8	-4.0/+2.1	-2.5/+1.6	-1.6/+1.2	-1.1/+0.9	-0.7/+0.6	-0.5/+0.5	-0.4/+0.3
.16	-14.8/+3.3	-6.5/+2.7	-3.8/+2.1	-2.4/+1.6	-1.6/+1.2	-1.0/+0.9	-0.7/+0.6	-0.5/+0.4	-0.3/+0.3
.17	-13.4/+3.2	-6.2/+2.6	-3.6/+2.0	-2.3/+1.5	-1.5/+1.1	-1.0/+0.8	-0.7/+0.6	-0.5/+0.4	-0.3/+0.3
.18	-12.2/+3.1	-5.8/+2.5	-3.4/+1.9	-2.2/+1.4	-1.4/+1.1	-1.0/+0.8	-0.7/+0.6	-0.5/+0.4	-0.3/+0.3
.19	-11.3/+3.0	-5.5/+2.4	-3.3/+1.8	-2.1/+1.4	-1.4/+1.0	-0.9/+0.8	-0.6/+0.5	-0.4/+0.4	-0.3/+0.3
.20	-10.5/+2.9	-5.2/+2.3	-3.1/+1.8	-2.0/+1.3	-1.3/+1.0	-0.9/+0.7	-0.6/+0.5	-0.4/+0.4	-0.3/+0.3
.21	-9.9/+2.8	-5.0/+2.2	-3.0/+1.7	-1.9/+1.3	-1.3/+1.0	-0.9/+0.7	-0.6/+0.5	-0.4/+0.4	-0.3/+0.3
.22	-9.3/+2.7	-4.8/+2.2	-2.9/+1.7	-1.8/+1.3	-1.2/+0.9	-0.8/+0.7	-0.6/+0.5	-0.4/+0.4	-0.3/+0.3
.23	-8.8/+2.7	-4.6/+2.1	-2.7/+1.6	-1.8/+1.2	-1.2/+0.9	-0.8/+0.7	-0.5/+0.5	-0.4/+0.3	-0.3/+0.2
.24	-8.3/+2.6	-4.4/+2.0	-2.6/+1.6	-1.7/+1.2	-1.1/+0.9	-0.8/+0.6	-0.5/+0.5	-0.4/+0.3	-0.3/+0.2
.25	-7.9/+2.5	-4.2/+2.0	-2.5/+1.5	-1.6/+1.1	-1.1/+0.8	-0.7/+0.6	-0.5/+0.4	-0.4/+0.3	-0.2/+0.2
.26	-7.5/+2.4	-4.0/+1.9	-2.4/+1.5	-1.6/+1.1	-1.0/+0.8	-0.7/+0.6	-0.5/+0.4	-0.3/+0.3	-0.2/+0.2
.27	-7.2/+2.4	-3.9/+1.9	-2.4/+1.4	-1.5/+1.1	-1.0/+0.8	-0.7/+0.6	-0.5/+0.4	-0.3/+0.3	-0.2/+0.2
.28	-6.8/+2.3	-3.7/+1.8	-2.3/+1.4	-1.5/+1.0	-1.0/+0.8	-0.7/+0.6	-0.5/+0.4	-0.3/+0.3	-0.2/+0.2
.29	-6.6/+2.2	-3.6/+1.7	-2.2/+1.3	-1.4/+1.0	-0.9/+0.7	-0.6/+0.5	-0.4/+0.4	-0.3/+0.3	-0.2/+0.2
.30	-6.3/+2.2	-3.5/+1.7	-2.1/+1.3	-1.4/+1.0	-0.9/+0.7	-0.6/+0.5	-0.4/+0.4	-0.3/+0.3	-0.2/+0.2
.31	-6.0/+2.1	-3.3/+1.7	-2.1/+1.3	-1.3/+0.9	-0.9/+0.7	-0.6/+0.5	-0.4/+0.4	-0.3/+0.3	-0.2/+0.2
.32	-5.8/+2.0	-3.2/+1.6	-2.0/+1.2	-1.3/+0.9	-0.9/+0.7	-0.6/+0.5	-0.4/+0.4	-0.3/+0.3	-0.2/+0.2
.33	-5.6/+2.0	-3.1/+1.6	-1.9/+1.2	-1.2/+0.9	-0.8/+0.7	-0.6/+0.5	-0.4/+0.3	-0.3/+0.2	-0.2/+0.2
.34	-5.4/+1.9	-3.0/+1.5	-1.9/+1.2	-1.2/+0.9	-0.8/+0.6	-0.6/+0.5	-0.4/+0.3	-0.3/+0.2	-0.2/+0.2
.35	-5.2/+1.9	-2.9/+1.5	-1.8/+1.1	-1.2/+0.8	-0.8/+0.6	-0.5/+0.5	-0.4/+0.3	-0.3/+0.2	-0.2/+0.2
.36	-5.0/+1.8	-2.8/+1.4	-1.7/+1.1	-1.1/+0.8	-0.8/+0.6	-0.5/+0.4	-0.4/+0.3	-0.2/+0.2	-0.2/+0.2
.37	-4.8/+1.8	-2.7/+1.4	-1.7/+1.1	-1.1/+0.8	-0.7/+0.6	-0.5/+0.4	-0.3/+0.3	-0.2/+0.2	-0.2/+0.2
.38	-4.6/+1.7	-2.6/+1.4	-1.6/+1.0	-1.1/+0.8	-0.7/+0.6	-0.5/+0.4	-0.3/+0.3	-0.2/+0.2	-0.2/+0.2
.39	-4.5/+1.7	-2.6/+1.3	-1.6/+1.0	-1.0/+0.8	-0.7/+0.6	-0.5/+0.4	-0.3/+0.3	-0.2/+0.2	-0.2/+0.1
.40	-4.3/+1.6	-2.5/+1.3	-1.5/+1.0	-1.0/+0.7	-0.7/+0.5	-0.5/+0.4	-0.3/+0.3	-0.2/+0.2	-0.2/+0.1
.41	-4.2/+1.6	-2.4/+1.3	-1.5/+1.0	-1.0/+0.7	-0.7/+0.5	-0.4/+0.4	-0.3/+0.3	-0.2/+0.2	-0.1/+0.1
.42	-4.0/+1.6	-2.3/+1.2	-1.4/+0.9	-0.9/+0.7	-0.6/+0.5	-0.4/+0.4	-0.3/+0.3	-0.2/+0.2	-0.1/+0.1
.43	-3.9/+1.5	-2.2/+1.2	-1.4/+0.9	-0.9/+0.7	-0.6/+0.5	-0.4/+0.4	-0.3/+0.3	-0.2/+0.2	-0.1/+0.1
.44	-3.8/+1.5	-2.1/+1.2	-1.4/+0.9	-0.9/+0.7	-0.6/+0.5	-0.4/+0.4	-0.3/+0.3	-0.2/+0.2	-0.1/+0.1
.45	-3.6/+1.4	-2.1/+1.1	-1.3/+0.9	-0.9/+0.6	-0.6/+0.5	-0.4/+0.3	-0.3/+0.2	-0.2/+0.2	-0.1/+0.1
.46	-3.5/+1.4	-2.0/+1.1	-1.3/+0.8	-0.8/+0.6	-0.6/+0.5	-0.4/+0.3	-0.3/+0.2	-0.2/+0.2	-0.1/+0.1
.47	-3.4/+1.4	-2.0/+1.1	-1.2/+0.8	-0.8/+0.6	-0.5/+0.4	-0.4/+0.3	-0.3/+0.2	-0.2/+0.2	-0.1/+0.1
.48	-3.3/+1.3	-1.9/+1.0	-1.2/+0.8	-0.8/+0.6	-0.5/+0.4	-0.4/+0.3	-0.3/+0.2	-0.2/+0.2	-0.1/+0.1
.49	-3.2/+1.3	-1.8/+1.0	-1.2/+0.8	-0.8/+0.6	-0.5/+0.4	-0.4/+0.3	-0.2/+0.2	-0.2/+0.2	-0.1/+0.1
.50	-3.1/+1.2	-1.8/+1.0	-1.1/+0.7	-0.7/+0.6	-0.5/+0.4	-0.3/+0.3	-0.2/+0.2	-0.2/+0.2	-0.1/+0.1

TABLE I. - Concluded.

(b) Concluded

Measured coherence	Number of samples, N								
	16	32	64	128	256	512	1024	2048	4096
	Confidence level, dB								
0.51	-3.0/+1.2	-1.7/+0.9	-1.1/+0.7	-0.7/+0.5	-0.5/+0.4	-0.3/+0.3	-0.2/+0.2	-0.2/+0.1	-0.1/+0.1
.52	-2.9/+1.2	-1.7/+0.9	-1.1/+0.7	-0.7/+0.5	-0.5/+0.4	-0.3/+0.3	-0.2/+0.2	-0.2/+0.1	-0.1/+0.1
.53	-2.8/+1.1	-1.6/+0.9	-1.0/+0.7	-0.7/+0.5	-0.5/+0.4	-0.3/+0.3	-0.2/+0.2	-0.1/+0.1	-0.1/+0.1
.54	-2.7/+1.1	-1.6/+0.9	-1.0/+0.7	-0.7/+0.5	-0.4/+0.4	-0.3/+0.3	-0.2/+0.2	-0.1/+0.1	-0.1/+0.1
.55	-2.6/+1.1	-1.5/+0.8	-1.0/+0.6	-0.6/+0.5	-0.4/+0.3	-0.3/+0.3	-0.2/+0.2	-0.1/+0.1	-0.1/+0.1
.56	-2.5/+1.0	-1.5/+0.8	-0.9/+0.6	-0.6/+0.5	-0.4/+0.3	-0.3/+0.2	-0.2/+0.2	-0.1/+0.1	-0.1/+0.1
.57	-2.4/+1.0	-1.4/+0.8	-0.9/+0.6	-0.6/+0.4	-0.4/+0.3	-0.3/+0.2	-0.2/+0.2	-0.1/+0.1	-0.1/+0.1
.58	-2.4/+1.0	-1.4/+0.8	-0.9/+0.6	-0.6/+0.4	-0.4/+0.3	-0.3/+0.2	-0.2/+0.2	-0.1/+0.1	-0.1/+0.1
.59	-2.3/+0.9	-1.3/+0.7	-0.8/+0.6	-0.6/+0.4	-0.4/+0.3	-0.3/+0.2	-0.2/+0.2	-0.1/+0.1	-0.1/+0.1
.60	-2.2/+0.9	-1.3/+0.7	-0.8/+0.5	-0.5/+0.4	-0.4/+0.3	-0.2/+0.2	-0.2/+0.2	-0.1/+0.1	-0.1/+0.1
.61	-2.1/+0.9	-1.2/+0.7	-0.8/+0.5	-0.5/+0.4	-0.4/+0.3	-0.2/+0.2	-0.2/+0.2	-0.1/+0.1	-0.1/+0.1
.62	-2.0/+0.9	-1.2/+0.7	-0.8/+0.5	-0.5/+0.4	-0.3/+0.3	-0.2/+0.2	-0.2/+0.1	-0.1/+0.1	-0.1/+0.1
.63	-2.0/+0.8	-1.2/+0.6	-0.7/+0.5	-0.5/+0.4	-0.3/+0.3	-0.2/+0.2	-0.2/+0.1	-0.1/+0.1	-0.1/+0.1
.64	-1.9/+0.8	-1.1/+0.6	-0.7/+0.5	-0.5/+0.4	-0.3/+0.3	-0.2/+0.2	-0.1/+0.1	-0.1/+0.1	-0.1/+0.1
.65	-1.8/+0.8	-1.1/+0.6	-0.7/+0.5	-0.5/+0.3	-0.3/+0.2	-0.2/+0.2	-0.1/+0.1	-0.1/+0.1	-0.1/+0.1
.66	-1.8/+0.7	-1.0/+0.6	-0.7/+0.4	-0.4/+0.3	-0.3/+0.2	-0.2/+0.2	-0.1/+0.1	-0.1/+0.1	-0.1/+0.1
.67	-1.7/+0.7	-1.0/+0.6	-0.6/+0.4	-0.4/+0.3	-0.3/+0.2	-0.2/+0.2	-0.1/+0.1	-0.1/+0.1	-0.1/+0.1
.68	-1.6/+0.7	-1.0/+0.5	-0.6/+0.4	-0.4/+0.3	-0.3/+0.2	-0.2/+0.2	-0.1/+0.1	-0.1/+0.1	-0.1/+0.1
.69	-1.6/+0.7	-0.9/+0.5	-0.6/+0.4	-0.4/+0.3	-0.3/+0.2	-0.2/+0.2	-0.1/+0.1	-0.1/+0.1	-0.1/+0.1
.70	-1.5/+0.6	-0.9/+0.5	-0.6/+0.4	-0.4/+0.3	-0.3/+0.2	-0.2/+0.1	-0.1/+0.1	-0.1/+0.1	-0.1/+0.1
.71	-1.4/+0.6	-0.9/+0.5	-0.5/+0.4	-0.4/+0.3	-0.2/+0.2	-0.2/+0.1	-0.1/+0.1	-0.1/+0.1	-0.1/+0.1
.72	-1.4/+0.6	-0.8/+0.5	-0.5/+0.3	-0.3/+0.3	-0.2/+0.2	-0.2/+0.1	-0.1/+0.1	-0.1/+0.1	-0.1/+0.1
.73	-1.3/+0.6	-0.8/+0.4	-0.5/+0.3	-0.3/+0.2	-0.2/+0.2	-0.2/+0.1	-0.1/+0.1	-0.1/+0.1	-0.1/+0.0
.74	-1.3/+0.5	-0.7/+0.4	-0.5/+0.3	-0.3/+0.2	-0.2/+0.2	-0.1/+0.1	-0.1/+0.1	-0.1/+0.1	-0.0/+0.0
.75	-1.2/+0.5	-0.7/+0.4	-0.5/+0.3	-0.3/+0.2	-0.2/+0.2	-0.1/+0.1	-0.1/+0.1	-0.1/+0.1	-0.0/+0.0
.76	-1.1/+0.5	-0.7/+0.4	-0.4/+0.3	-0.3/+0.2	-0.2/+0.2	-0.1/+0.1	-0.1/+0.1	-0.1/+0.1	-0.0/+0.0
.77	-1.1/+0.5	-0.6/+0.4	-0.4/+0.3	-0.3/+0.2	-0.2/+0.2	-0.1/+0.1	-0.1/+0.1	-0.1/+0.1	-0.0/+0.0
.78	-1.0/+0.4	-0.6/+0.3	-0.4/+0.3	-0.3/+0.2	-0.2/+0.1	-0.1/+0.1	-0.1/+0.1	-0.1/+0.1	-0.0/+0.0
.79	-1.0/+0.4	-0.6/+0.3	-0.4/+0.2	-0.2/+0.2	-0.2/+0.1	-0.1/+0.1	-0.1/+0.1	-0.1/+0.1	-0.0/+0.0
.80	-0.9/+0.4	-0.6/+0.3	-0.4/+0.2	-0.2/+0.2	-0.2/+0.1	-0.1/+0.1	-0.1/+0.1	-0.1/+0.0	-0.0/+0.0
.81	-0.9/+0.4	-0.5/+0.3	-0.3/+0.2	-0.2/+0.2	-0.1/+0.1	-0.1/+0.1	-0.1/+0.1	-0.0/+0.0	-0.0/+0.0
.82	-0.8/+0.4	-0.5/+0.3	-0.3/+0.2	-0.2/+0.2	-0.1/+0.1	-0.1/+0.1	-0.1/+0.1	-0.0/+0.0	-0.0/+0.0
.83	-0.8/+0.3	-0.5/+0.3	-0.3/+0.2	-0.2/+0.1	-0.1/+0.1	-0.1/+0.1	-0.1/+0.1	-0.0/+0.0	-0.0/+0.0
.84	-0.7/+0.3	-0.4/+0.2	-0.3/+0.2	-0.2/+0.1	-0.1/+0.1	-0.1/+0.1	-0.1/+0.1	-0.0/+0.0	-0.0/+0.0
.85	-0.7/+0.3	-0.4/+0.2	-0.3/+0.2	-0.2/+0.1	-0.1/+0.1	-0.1/+0.1	-0.1/+0.0	-0.0/+0.0	-0.0/+0.0
.86	-0.6/+0.3	-0.4/+0.2	-0.2/+0.2	-0.2/+0.1	-0.1/+0.1	-0.1/+0.1	-0.1/+0.0	-0.0/+0.0	-0.0/+0.0
.87	-0.6/+0.3	-0.3/+0.2	-0.2/+0.1	-0.1/+0.1	-0.1/+0.1	-0.1/+0.1	-0.0/+0.0	-0.0/+0.0	-0.0/+0.0
.88	-0.5/+0.2	-0.3/+0.2	-0.2/+0.1	-0.1/+0.1	-0.1/+0.1	-0.1/+0.1	-0.0/+0.0	-0.0/+0.0	-0.0/+0.0
.89	-0.5/+0.2	-0.3/+0.2	-0.2/+0.1	-0.1/+0.1	-0.1/+0.1	-0.1/+0.0	-0.0/+0.0	-0.0/+0.0	-0.0/+0.0
.90	-0.4/+0.2	-0.3/+0.1	-0.2/+0.1	-0.1/+0.1	-0.1/+0.1	-0.1/+0.0	-0.0/+0.0	-0.0/+0.0	-0.0/+0.0
.91	-0.4/+0.2	-0.2/+0.1	-0.1/+0.1	-0.1/+0.1	-0.1/+0.1	-0.0/+0.0	-0.0/+0.0	-0.0/+0.0	-0.0/+0.0
.92	-0.3/+0.2	-0.2/+0.1	-0.1/+0.1	-0.1/+0.1	-0.1/+0.0	-0.0/+0.0	-0.0/+0.0	-0.0/+0.0	-0.0/+0.0
.93	-0.3/+0.1	-0.2/+0.1	-0.1/+0.1	-0.1/+0.1	-0.1/+0.0	-0.0/+0.0	-0.0/+0.0	-0.0/+0.0	-0.0/+0.0
.94	-0.3/+0.1	-0.2/+0.1	-0.1/+0.1	-0.1/+0.0	-0.0/+0.0	-0.0/+0.0	-0.0/+0.0	-0.0/+0.0	-0.0/+0.0
.95	-0.2/+0.1	-0.1/+0.1	-0.1/+0.1	-0.1/+0.0	-0.0/+0.0	-0.0/+0.0	-0.0/+0.0	-0.0/+0.0	-0.0/+0.0
.96	-0.2/+0.1	-0.1/+0.1	-0.1/+0.0	-0.0/+0.0	-0.0/+0.0	-0.0/+0.0	-0.0/+0.0	-0.0/+0.0	-0.0/+0.0
.97	-0.1/+0.1	-0.1/+0.0	-0.0/+0.0	-0.0/+0.0	-0.0/+0.0	-0.0/+0.0	-0.0/+0.0	-0.0/+0.0	-0.0/+0.0
.98	-0.1/+0.0	-0.0/+0.0	-0.0/+0.0	-0.0/+0.0	-0.0/+0.0	-0.0/+0.0	-0.0/+0.0	-0.0/+0.0	-0.0/+0.0
.99	-0.0/+0.0	-0.0/+0.0	-0.0/+0.0	-0.0/+0.0	-0.0/+0.0	-0.0/+0.0	-0.0/+0.0	-0.0/+0.0	-0.0/+0.0

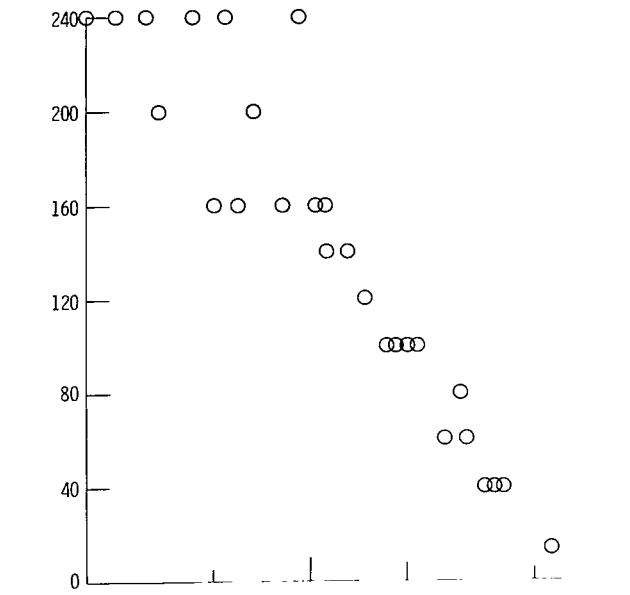

(a) Low coherence tone; experimental data taken at low (cutoff) speed.

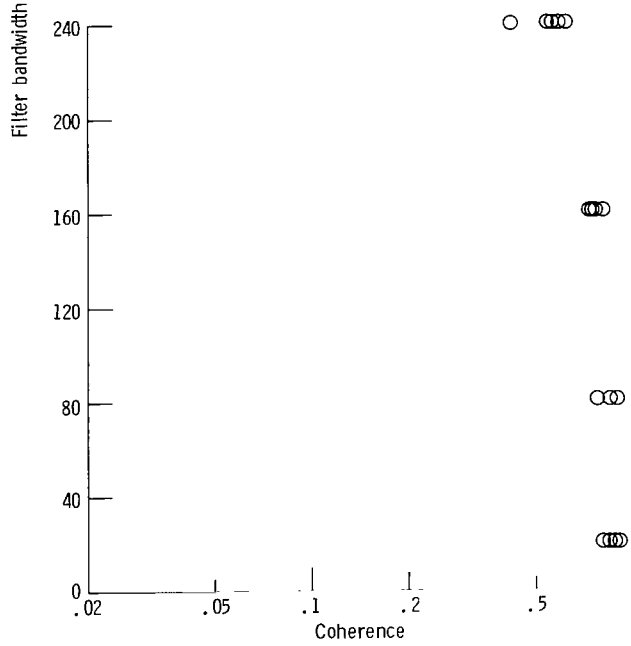

(b) High coherence tone; experimental data taken at high (cuton) speed.

Figure 1. - Coherence trends with bandwidth.

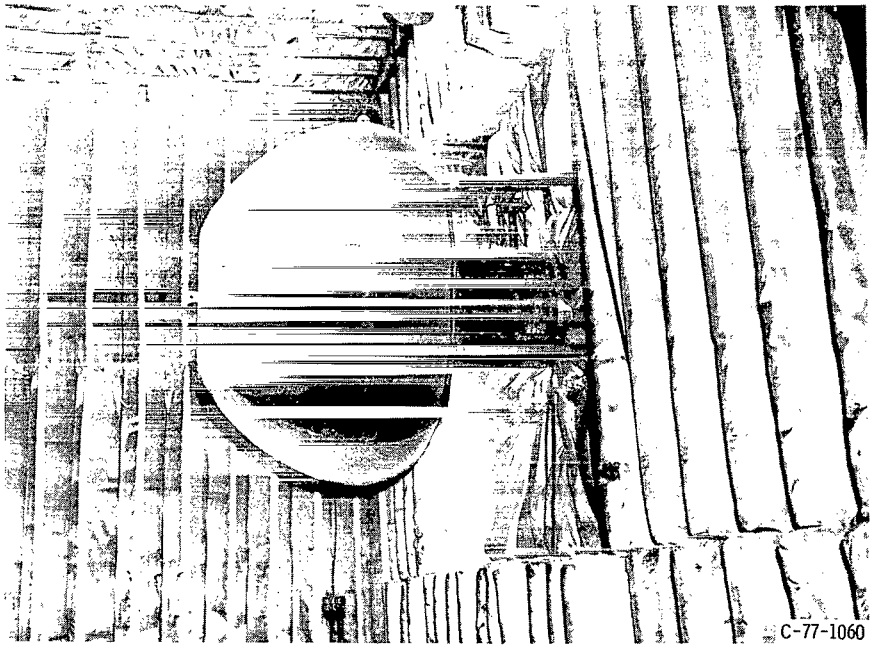

(a) With inflow control.

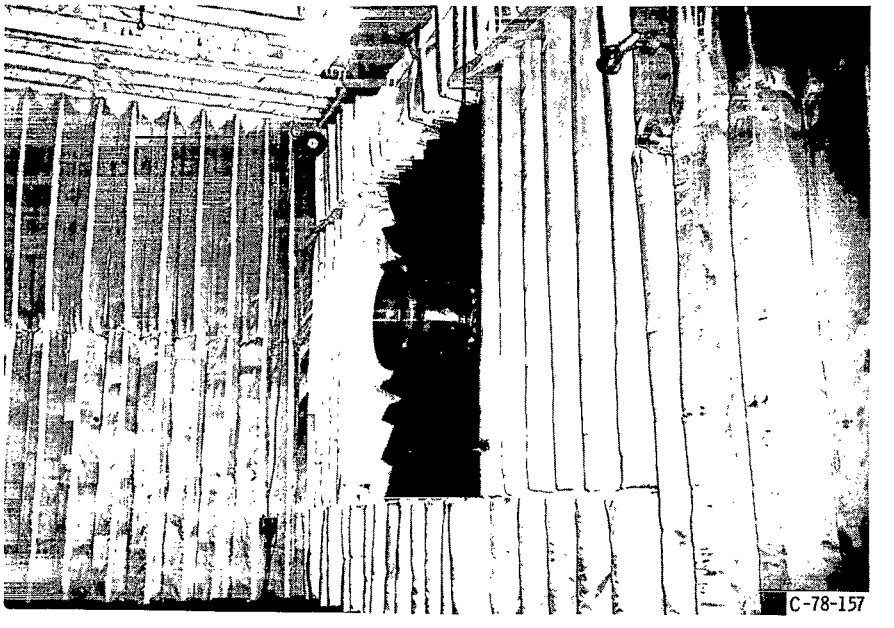

(b) Without inflow control.

Figure 2. - Views of fan inlet.

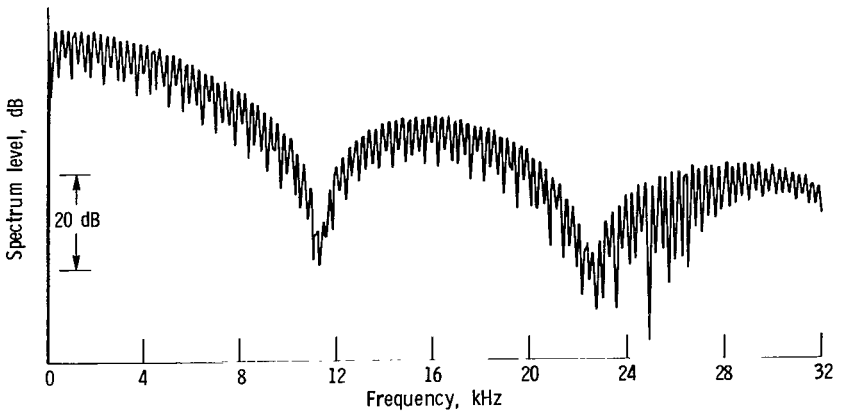

Figure 3. - Spectrum of fan speed signal showing shaft rate harmonics.

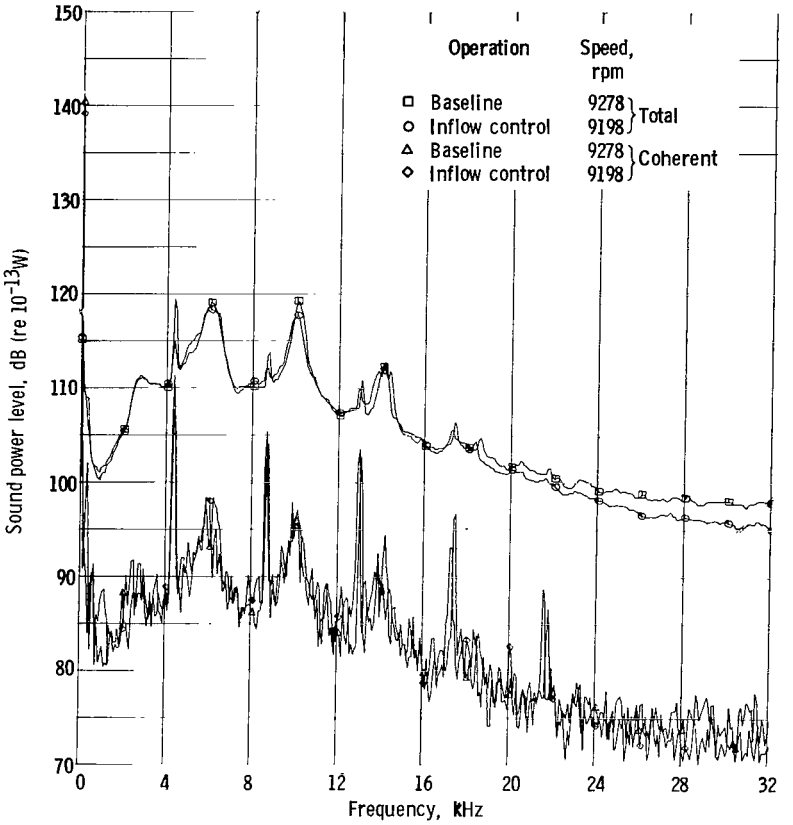

Figure 4. - Total and coherent power spectra at 50 percent of design speed.

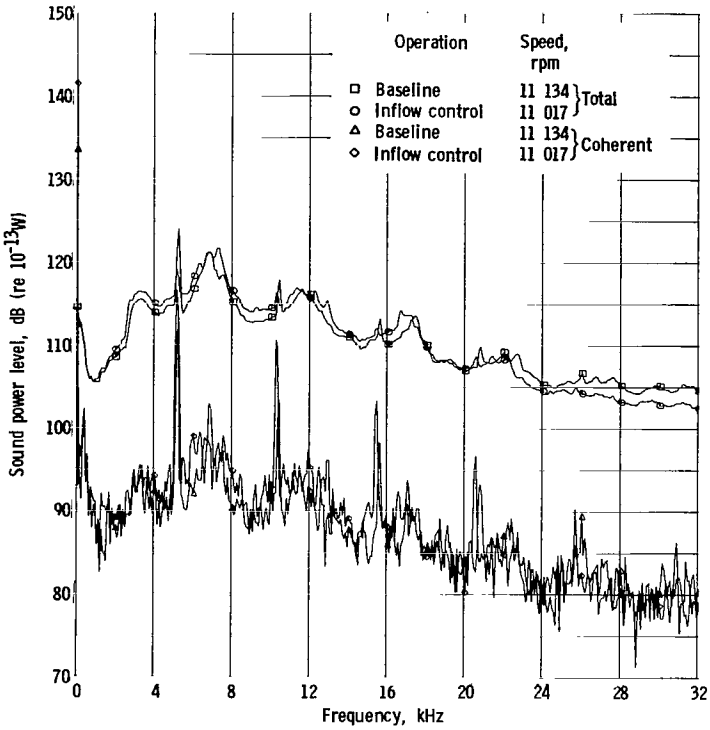

Figure 5. - Total and coherent power spectra at 60 percent of design speed.

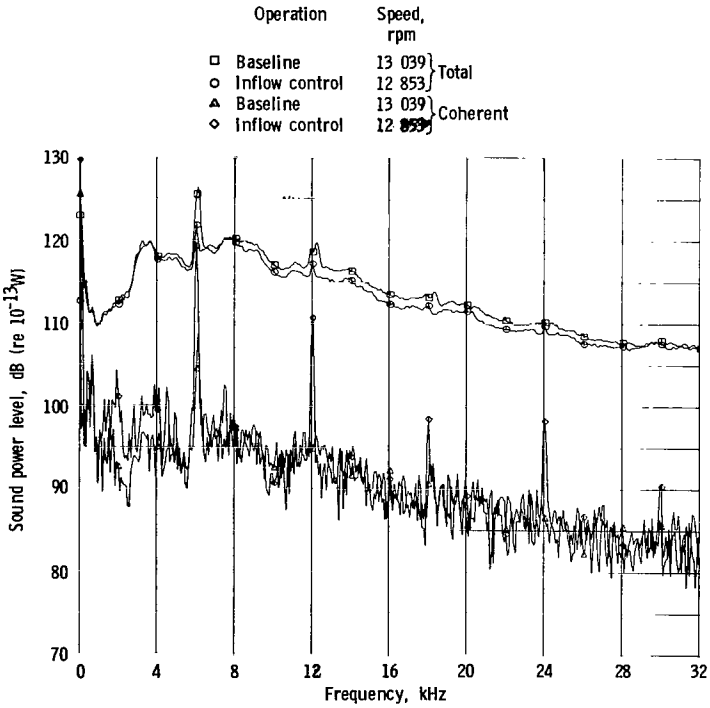

Figure 6. - Total and coherent power spectra at 70 percent of design speed.

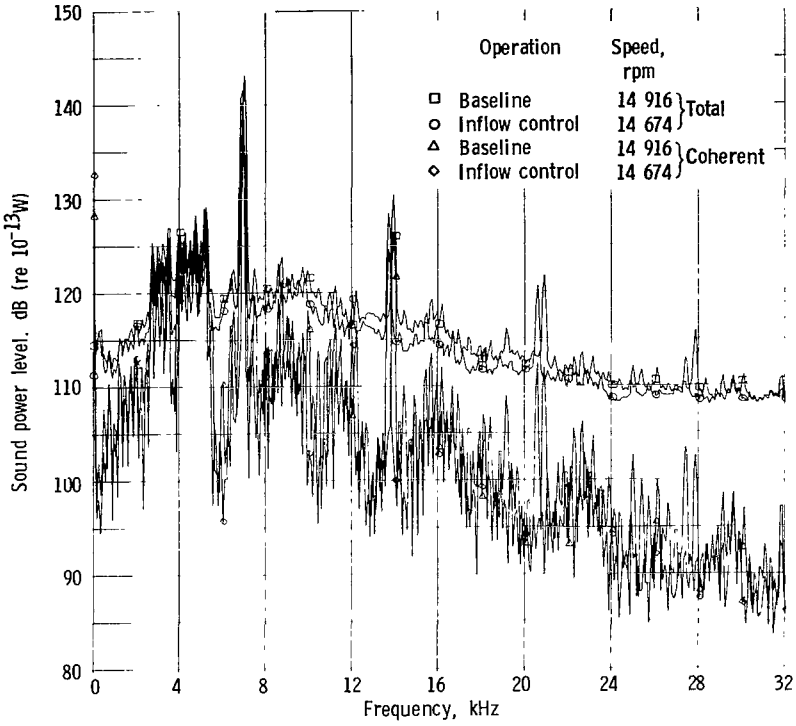

Figure 7. - Total and coherent power spectra at 80 percent of design speed.

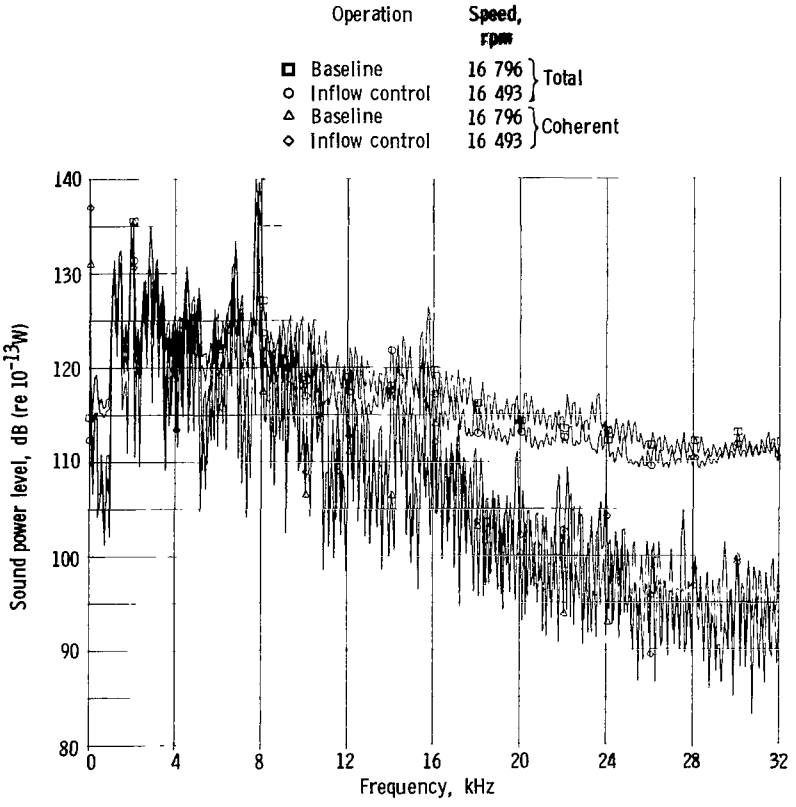

Figure 8. - Total and coherent power spectra at 90 percent of design speed.

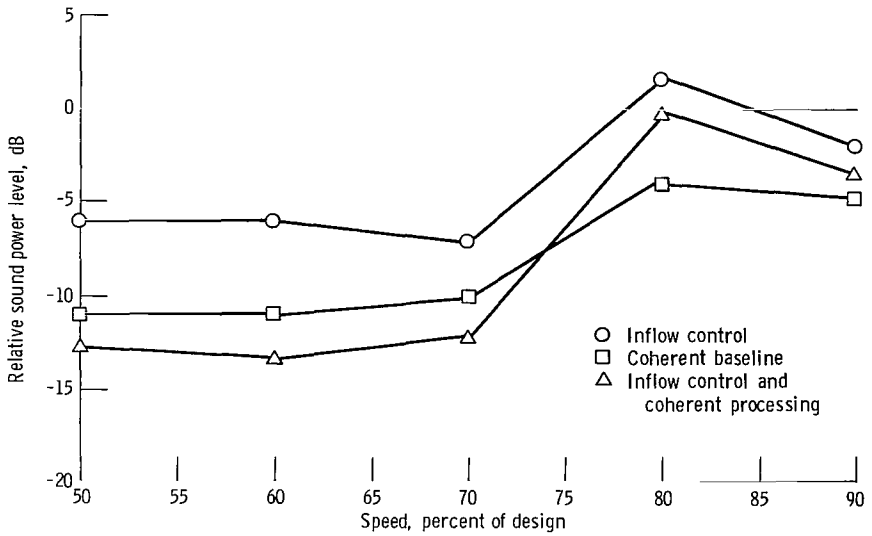

Figure 9. - QF-12 sound power levels of BPF tone for inflow control and coherent baseline relative to baseline - survey microphone.

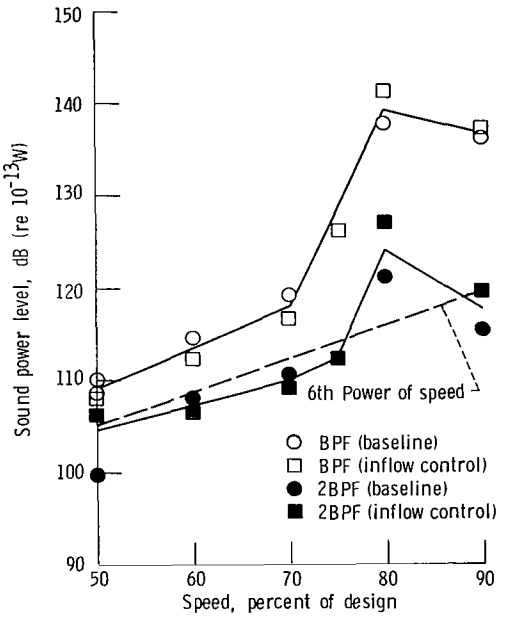

Figure 10. - Fan coherent sound power levels.

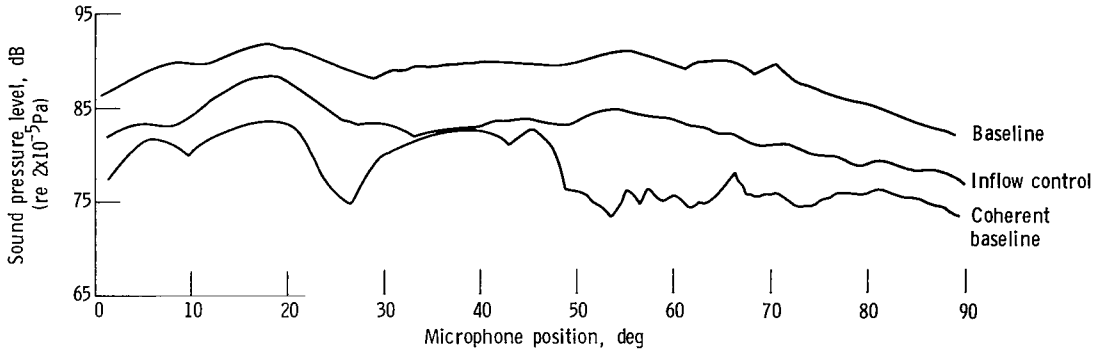

Figure 11. - Blade-passing-frequency tone directivity at 50 percent of design speed.

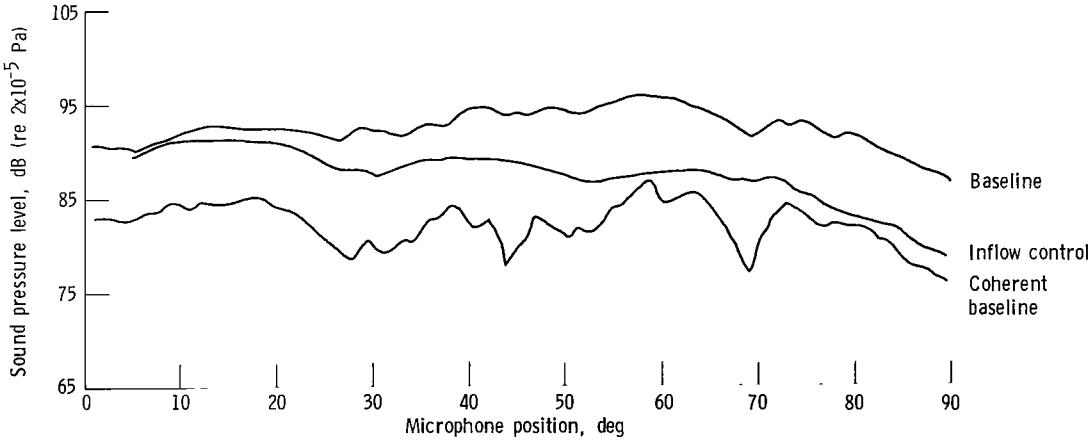

Figure 12. - Blade-passing-frequency tone directivity at 60 percent of design speed.

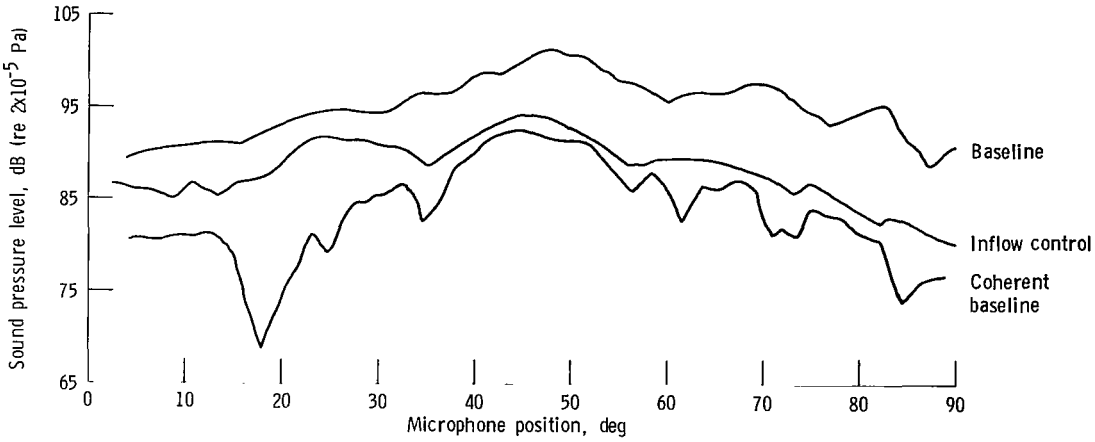

Figure 13. - Blade-passing-frequency tone directivity at 70 percent of design speed.

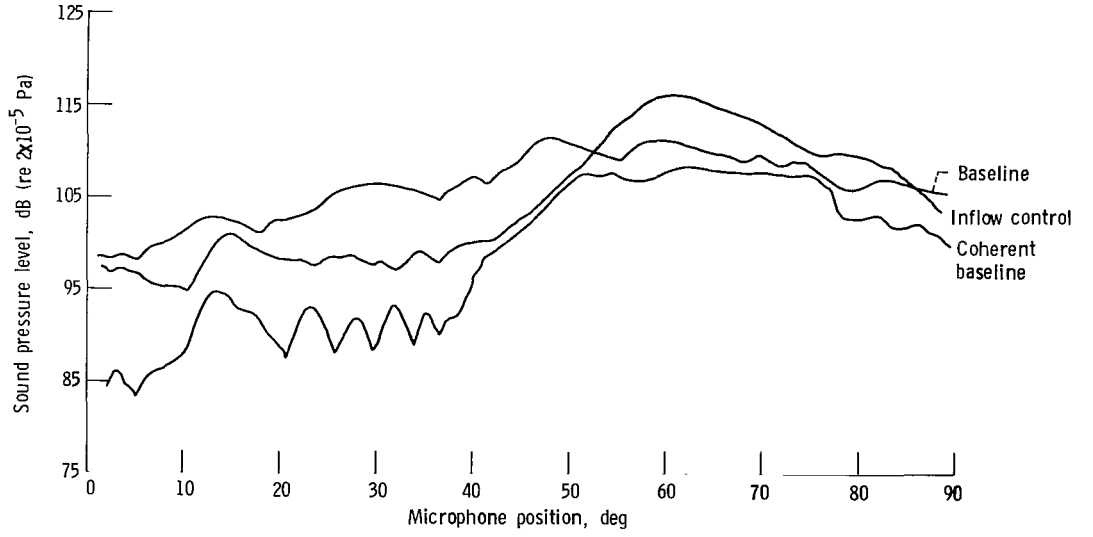

Figure 14. - Blade-passing-frequency tone directivity at 80 percent of design speed.

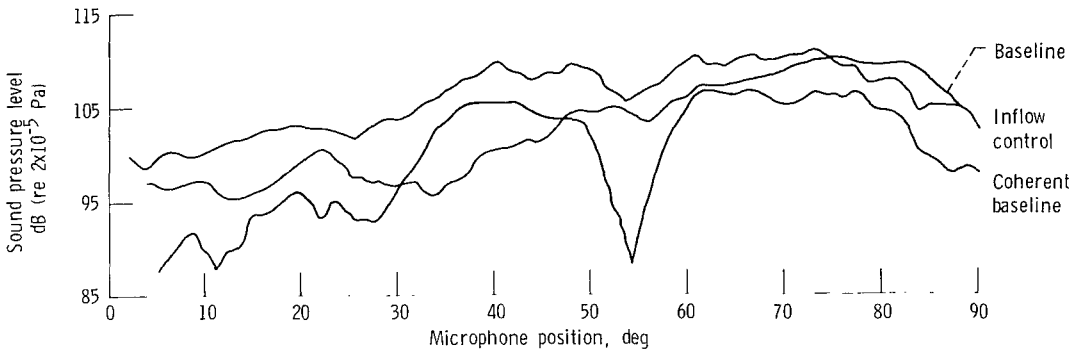

Figure 15. - Blade-passing-frequency tone directivity at 90 percent of design speed.

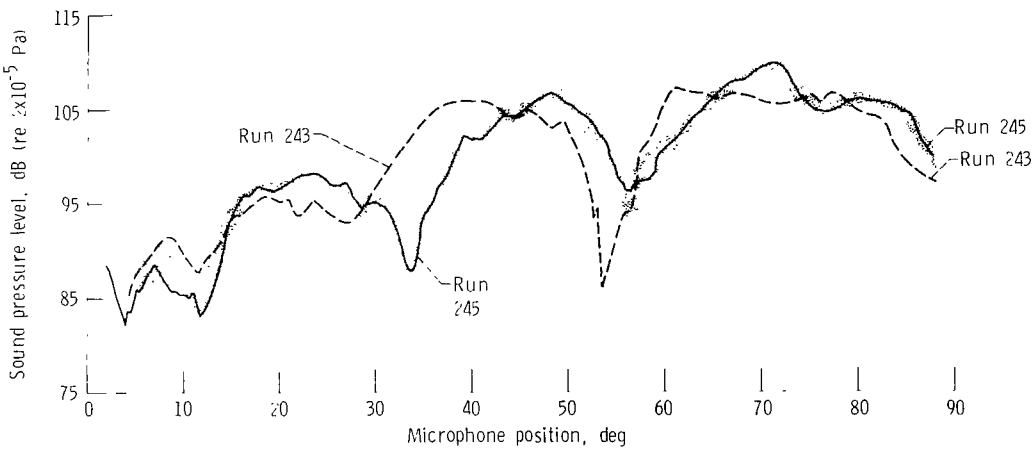

Figure 16. - Blade-passing-frequency distribution for similar runs showing 90 percent confidence limits. Speed, 90 percent of design; survey microphone; baseline condition.

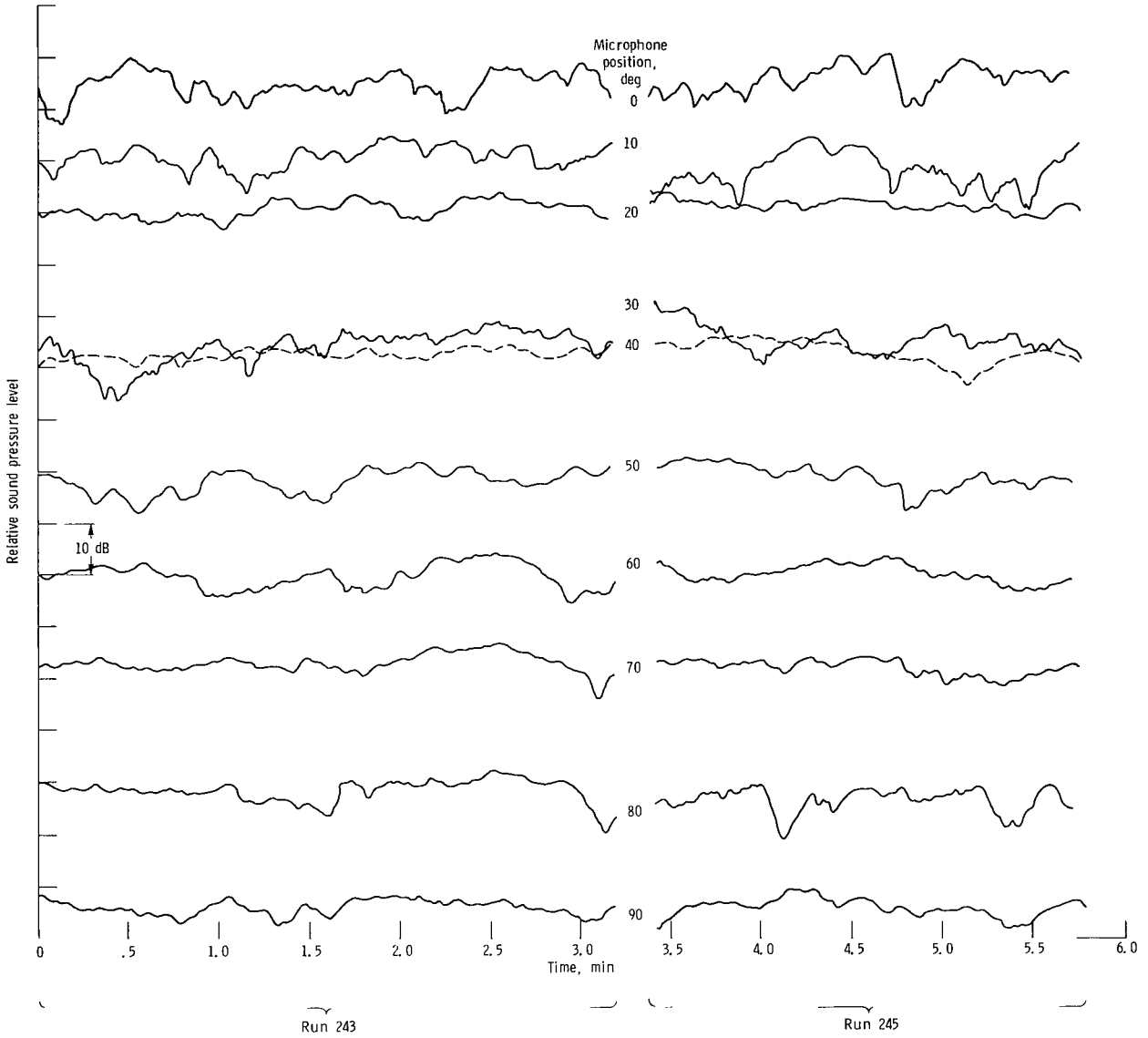

Figure 17. - Time history of baseline coherent BPF tone at 90 percent of design speed.

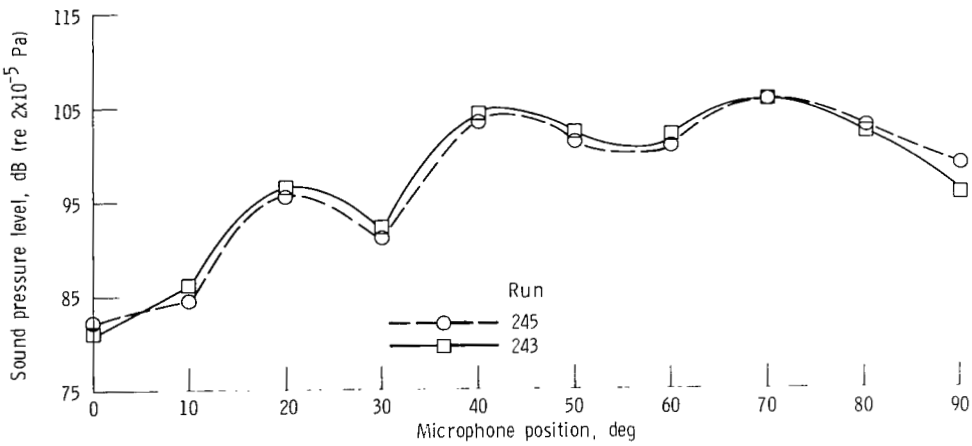

Figure 18. - Blade-passing-frequency tone directivity for similar runs after averaging. Speed, 90 percent of design; fixed microphones; baseline condition.

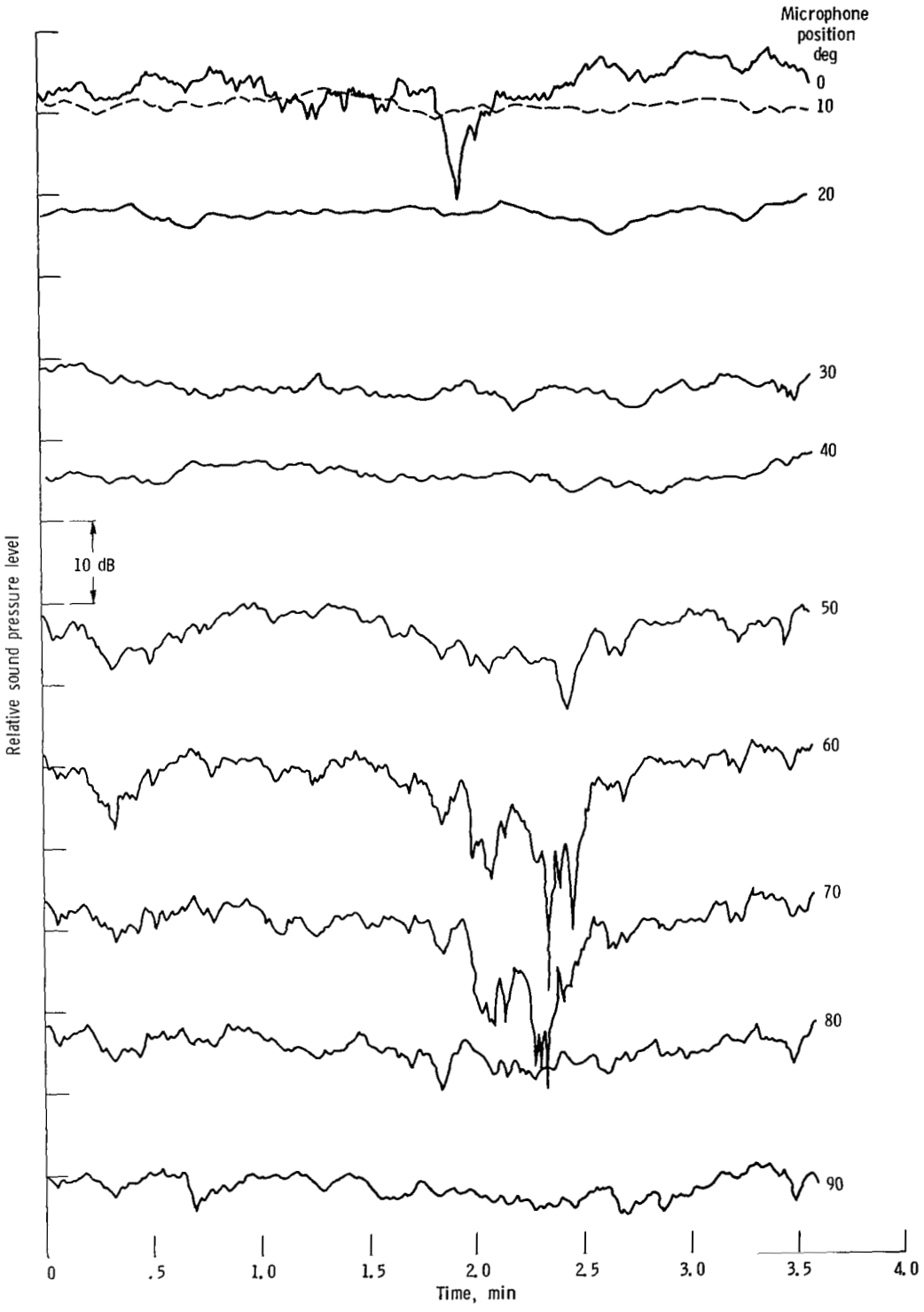

Figure 19. - Time history of baseline coherent blade-passing-frequency tone at 50 percent of design speed.

1. Report No. NASA TP-1630	2. Government Accession No.	3. Recipient's Catalog No.
4. Title and Subtitle APPLICATION OF COHERENCE IN FAN NOISE STUDIES		5. Report Date February 1980 6. Performing Organization Code
7. Author(s) Joseph R. Balombin		8. Performing Organization Report No. E-157 10. Work Unit No. 505-03
9. Performing Organization Name and Address National Aeronautics and Space Administration Lewis Research Center Cleveland, Ohio 44135		11. Contract or Grant No. 13. Type of Report and Period Covered Technical Paper
12. Sponsoring Agency Name and Address National Aeronautics and Space Administration Washington, D.C. 20546		14. Sponsoring Agency Code

15. Supplementary Notes

16. Abstract

A study of fan noise has been made by using the coherence function to obtain far-field spectra that were coherent with the fan rotational rate. Choosing fan rotational rate as one of the two variables has yielded new information about the far-field noise generated during static fan testing. As a result of this coherent data processing, the inlet fan-tone noise present in static testing was determined to be mostly random when the rotor-alone and rotor-stator interaction tones were cut off. After the rotor-alone sound field was cut on, the sound pressure became coherent, and the angular extent of high coherence increased as fan speed was increased. In addition, the sound field was organized as a pattern of lobes whose amplitude varied slowly with time. Additional fan test results indicate that operating the fan with an inflow control device can partially reduce the fan-tone noise levels to those produced by coherent processing.

17. Key Words (Suggested by Author(s))	18. Distribution Statement
Acoustics; Fan noise; Inlet distortion; Inlet turbulence; Sound pressure	Unclassified - unlimited STAR Category 71

19. Security Classif. (of this report)	20. Security Classif. (of this page)	21. No. of Pages	22. Price*
Unclassified	Unclassified	25	A02

* For sale by the National Technical Information Service, Springfield, Virginia 22161

NASA-Langley, 1980

9 1 1U,H, 020880 S00903DS
DEPT OF THE AIR FORCE
AF WEAPONS LABORATORY
ATTN: TECHNICAL LIBRARY (SUL)
KIRTLAND AFB NM 87117